

Article

Hybrid (Oscillator-Amplifier) Free Electron Laser and New Proposals

Andrea Doria

ENEA, Fusion Physics Division, C.R. Frascati, via E. Fermi 45, I-00044 Frascati (Rome), Italy; andrea.doria@enea.it

Abstract: The present work analyses a hybrid free electron laser (FEL) scheme where the oscillator is based on a radiation source operating with a slow-wave guiding structure as, for instance, a Cerenkov FEL or a Smith–Purcell FEL. Such devices, often running in transverse magnetic (TM) modes, present a longitudinal electric field which can easily affect the longitudinal electrons' velocities, inducing an energy modulation on the beam. Such a modulation, properly controlled, can induce a strong radiation emission in a magnetic undulator properly designed to operate as a radiator. General considerations will be exposed together with a practical numerical example in the far infrared region of the spectrum.

Keywords: free electron laser; Oscillator-Amplifier; TeraHertz



Citation: Doria, A. Hybrid (Oscillator-Amplifier) Free Electron Laser and New Proposals. *Appl. Sci.* **2021**, *11*, 5948. <https://doi.org/10.3390/app11135948>

Academic Editors: Giuseppe Dattoli, Alessandro Curcio and Danilo Giulietti

Received: 25 May 2021
Accepted: 22 June 2021
Published: 26 June 2021

Publisher's Note: MDPI stays neutral with regard to jurisdictional claims in published maps and institutional affiliations.



Copyright: © 2021 by the author. Licensee MDPI, Basel, Switzerland. This article is an open access article distributed under the terms and conditions of the Creative Commons Attribution (CC BY) license (<https://creativecommons.org/licenses/by/4.0/>).

1. Introduction

Free electron lasers (FELs) are widely acknowledged as the most versatile generators of coherent electromagnetic radiation. Since the first studies in the late 1960s [1] and their “official” invention in 1977 [2], it has been clear that FELs are capable of bridging the gap between conventional electron-based sources (such as klystrons, magnetrons, travelling wave tubes) that are limited to the high frequency direction, and the lasers that, with some exceptions, generate single frequency radiation with a power that is limited by the nature of the active medium. FELs can be designed, in principle, to operate at any frequency and with a time structure and related power suitable for any kind of experiment. This kind of flexibility comes from the fact that many of the parameters involved, such as the electron energy and the magnetic field, can be adjusted with continuity. Moreover, many dynamical regimes can be exploited for FEL design; from the low-gain regime, suitable for oscillator devices [3], to the high gain regime ideal for the self-amplified spontaneous emission (SASE) scheme [4]. Furthermore, FEL offers significant potential options to combine different schemes in sequence in order to increase the performances of some specific features without overly stressing the project parameters. One of the most relevant FEL structures arrangements, among others, is a modulator at a synchronous frequency followed by a frequency multiplier that exploits the harmonic content in the modulated beam [5,6]. Such an arrangement may be reproduced several times, creating a kind of cascade [7] that results in final beam degradation.

This study presents one of the possible arrangements based on a Cerenkov FEL oscillator as a modulator and a magnetic undulator as a radiator: this solution can be considered a hybrid FEL scheme device [8]. The reason why the term hybrid can be ascribed to such a scheme is not only due to the fact that the modulator and radiator present two different mechanisms of radiation generation, but mainly because in Cerenkov-like FEL devices [9] (as is the case for Smith–Purcell gratings [10]), the coupling between electrons and field is longitudinal, while the magnetic undulator induces a transverse motion to the electrons and accordingly, to the coupling. This circumstance, combined with the fact that Cerenkov (and Smith–Purcell) FELs operate with slow-wave guiding structures, has a relevant effect on the differences, for “synchronism condition” [9,11],

that links the spontaneous emission wavelength with the most relevant parameters of the experiment, between Cerenkov and undulator FELs.

The paper is arranged in four sections: after the present Introduction, Section 2 is dedicated to the study of the Cerenkov-based modulator. Section 3 will introduce the hybrid system as a whole, highlighting the value of the main parameters. Section 4 will describe the effects of the modulation on the emission from a magnetic undulator exploited as a radiator; this analysis includes the ballistic effects of a variable drift space. Section 5 is devoted to final conclusions.

2. The Hybrid System

The hybrid FEL system can be assumed to be composed of three main elements: (1) an electron beam accelerator; (2) a Cerenkov slow-wave guiding structure, with an adequate radiation resonator for the saturation regime accomplishment; and lastly, (3) a magnetic undulator acting as a radiator after the velocity modulation induced by an electric field associated with the radiation stored in the Cerenkov oscillator (see Figure 1).

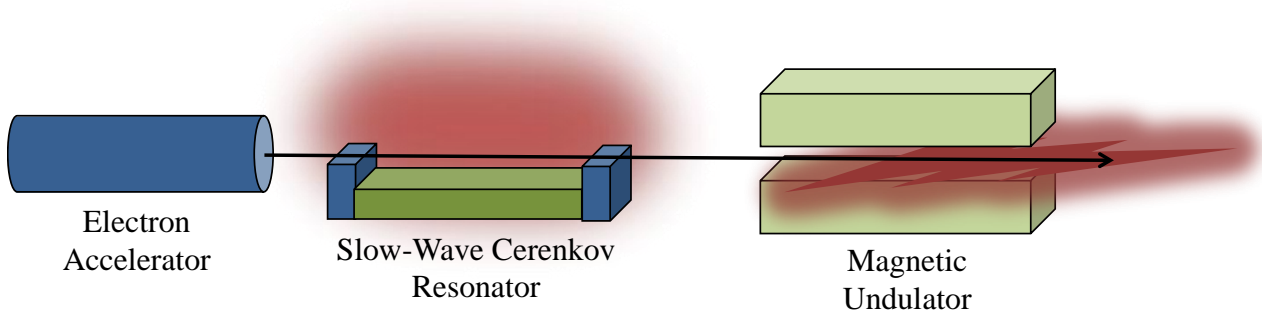


Figure 1. Schematic drawing of the hybrid FEL under study. The accelerated electron beam generates radiation interacting with the Cerenkov resonator. The electric beam associated with the stored radiation modulates the electrons' velocities in order to obtain the most efficient emission in the magnetic undulator radiator.

The first problem to face is related to the energy of the electron beam that will be common to both generating structures. As discussed in the introduction, the synchronism conditions for Cerenkov and undulator FELs are rather different and can be summarised as follows (see Refs. [9,11]), where the subscript U and C indicate the undulator and Cerenkov, respectively:

$$\lambda_U = \frac{\lambda_w}{2\gamma^2} (1 + K^2); \lambda_C = 2\pi\gamma d \left(\frac{\epsilon - 1}{\epsilon} \right) \quad (1)$$

where λ_w indicates the undulator period, K is the undulator parameter, d is the dielectric thickness of the Cerenkov guiding structure, ϵ is its dielectric constant and γ is the Lorentz parameter of the electrons. All these parameters will be more deeply described in the following sections.

In order to obtain an efficient modulation of the electron beam, it is required that the radiation generated from the Cerenkov oscillator and from the Undulator radiator be "correlated"; a way to achieve this target is to obtain the condition: $\lambda_U = \lambda_C/n$ where $n = 1, 2, \dots$ specifies the harmonic number. Such a relation, with the use of Equation (1), becomes:

$$\frac{\lambda_w}{2\gamma^2} (1 + K^2) = \frac{2\pi\gamma}{n} d \left(\frac{\epsilon - 1}{\epsilon} \right) \Leftrightarrow \gamma^3 = \frac{\lambda_w}{4\pi} n (1 + K^2) \frac{\epsilon}{d(\epsilon - 1)} \quad (2)$$

Equation (2) gives the value of the electron energy as a function of all the parameters involved in both the Cerenkov and undulator FELs. In order to have an idea about the numbers, we can assign some reasonable values for the involved parameters in Equation (2) such as: $\lambda_w = 2.5$ cm, $K = 1$, $d = 5$ μ m, $n = 1$, $\epsilon = 5$ (dielectric constant of quartz [12]) from

which we obtain a result, for the electron energy, $\gamma \sim 10$, that corresponds to a moderate relativistic energy. By inserting these values into Equation (1), we conclude that such a source would operate in the so-called far-infrared (FIR) spectral region (also called TeraHertz (THz)-region) because $\lambda_U \sim \lambda_C \sim 250 \mu\text{m}$.

Another approach can be obtained by rearranging Equation (2) as follows:

$$d \left(\frac{\epsilon - 1}{\epsilon} \right) = \frac{\lambda_w}{4\pi\gamma^3} (1 + K^2) n \tag{3}$$

from which it is possible to obtain the Cerenkov parameters values starting from the undulator FEL ones. Let us suppose we have an FEL source with $\lambda_w = 2.5 \text{ cm}$, $K = 1$, $\gamma = 20$ and again working on the fundamental harmonic $n = 1$, Equation (3) gives: $[d(\epsilon - 1)/\epsilon] \sim 5 \cdot 10^{-7} \mu\text{m}$. Such a value may be obtained in several ways since, for instance, $\epsilon = 2$ and $d = 1 \mu\text{m}$. Using all these values for the hybrid FEL parameters, we eventually obtain from Equation (1) the value for the emitted wavelength from both the elements of the hybrid FEL: $\lambda_U \sim \lambda_C \sim 60 \mu\text{m}$.

3. The Cerenkov FEL Oscillator

A well-known class of waveguides is characterised by having open boundaries and the possible presence of an electromagnetic (e.m.) field outside the boundary; these guides support propagating modes called “surface waves” [13]. Dielectric films deposited over conducting plates are devices that fall into the aforementioned category; the surface waves, in this case, present an exponential behaviour, normal to the dielectric surface, that decays when moving away. Such a waveguide category is the relevant one for the realisation of the Cerenkov FEL device because the field–particle interaction occurs in the region of the space where the “evanescent” e.m. field is present.

These propagating devices present field distributions associable with transverse electric (TE) or transverse magnetic (TM) modes. The case of TM modes is more favourable for the FEL use due to the presence of a longitudinal electric field component related to them. The vector potential for the TM modes of a single slab geometry waveguide is expressed by [9,13]

$$\begin{cases} A_x = A_0 \frac{ck}{\omega q} e^{-qx} \sin(kz) e^{-i\omega t} \\ A_y = 0 \\ A_z = A_0 \frac{c}{i\omega} e^{-qx} \sin(kz) e^{-i\omega t} \end{cases} \tag{4}$$

where k indicates the longitudinal momentum, while q is the transverse momentum in vacuum and p is the transverse momentum in the dielectric of thickness d . All these parameters are linked by two coupled “dispersion relations” that can be deduced by the field continuity along the vacuum–dielectric interface and dielectric–conductor interface:

$$\begin{cases} qd = \frac{pd}{\epsilon} \tan(pd) \\ (pd)^2 + (qd)^2 = d^2 \left(\frac{\omega}{c} \right)^2 (\epsilon - 1) \end{cases} \text{ and } \begin{cases} p = \sqrt{\epsilon \left(\frac{\omega}{c} \right)^2 - k^2} \\ q = \sqrt{k^2 - \left(\frac{\omega}{c} \right)^2} \end{cases} \tag{5}$$

In order to obtain the electric and magnetic fields from Equation (4), we can adopt the Coulomb gauge ($\mathbf{E} = -\partial\mathbf{A}/\partial t$; $\mathbf{B} = \nabla \times \mathbf{A}$) which is useful for evaluating the fields in absence of charges and currents, as for the free modes in a guiding structure. Neglecting the coupling between the electrons and the transverse electric field E_x (due to the small values of the electrons’ velocities in the x direction), we obtain for the longitudinal field:

$$E_z = -cA_0 e^{-qx} \sin(kz) e^{-i\omega t} \tag{6}$$

In order to achieve the maximum field intensity, it is necessary to reach the saturation regime inside the Cerenkov waveguide resonator. The dynamics of the emission process in Cerenkov FEL has been established in the past as far as the spontaneous emission process [9,14] is concerned and with regard to the stimulated emission mechanism and

the gain coefficient calculation [14,15]. Let us, therefore, consider the case discussed in Section 2 while discussing Equation (2); the relevant parameters are summarised in Table 1.

Table 1. Cerenkov FEL Parameters @ $\lambda = 250 \mu\text{m}$.

Cerenkov FEL Parameters @ $\lambda = 250 \mu\text{m}$					
Electron Energy	Dielectric Thickness	Dielectric Constant	Resonator Length	Resonator Width	Double Slab Height
$\gamma = 10.0$	$d = 50 \mu\text{m}$	$\epsilon = 5.0$	$L = 35.0 \text{ cm}$	$W = 1.0 \text{ cm}$	$D = 2 \text{ cm}$

Table 1 reports the parameters for both a single slab geometry device [9] and for the double slab one [16] adequate for an operation around $\lambda_C = 250 \mu\text{m}$. The behaviour of the spontaneous emission for a single-electron beam with a transverse size of $\sigma_x = 1 \text{ mm}$ (r.m.s.), as a function of frequency and beam centroid distance from the dielectric surface, is reported in Figure 2a). The same analysis for the double slab geometry and a beam size of $\sigma_x = 1 \text{ cm}$ (r.m.s.) is reported in Figure 2b):

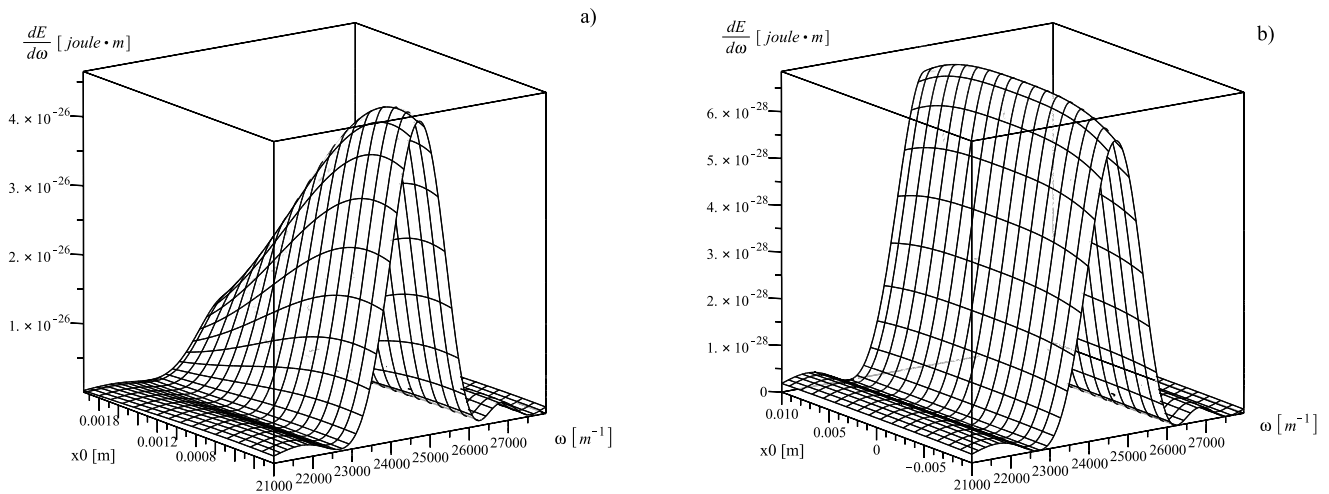


Figure 2. Spontaneous emission spectra as a function of the beam centroid distance from the dielectric surface: (a) single slab waveguide geometry; and (b) double slab waveguide geometry.

The one-dimensional stimulated emission process, until saturation, can be studied by means of semi-analytical techniques [17] (three-dimensional theory can be found in [18]). The saturation mechanism in free electron devices is quite similar to that occurring in conventional lasers, as has been derived by Rigrod approximately sixty years ago [19] and is also present in the theory of passive saturable absorber for laser mode-locking [20]. Two different but similar approaches can be applied; the first technique starts from the application of the Ginzburg–Landau equation to FEL systems [21] and leads to the $G_I(I)$ expression in Equation (7). The second method is based on the logistic equation approach [22] and ends up the $G_{II}(I)$ expression in Equation (7):

$$\left\{ \begin{array}{l} G_I(I_n) = 0.849 \cdot g_{0MAX} \frac{1 - \exp\left(-\frac{\pi}{2} \frac{I_n}{I_{SAT}}\right)}{\frac{\pi}{2} \frac{I_n}{I_{SAT}}} \\ I_{SAT} = \frac{\gamma I_0 I_{AV}}{4 g_{0MAX} N_{eq} c} \\ I_{n+1} = [I_n + G_I(I_n) I_n] (1 - \Gamma) \end{array} \right. ; \left\{ \begin{array}{l} G_{II}(n) = \frac{I(n) - I(n-1)}{I(n-1)} \\ I(n) = I_{SP} \frac{\exp\{[g_{0MAX}(1-\Gamma) - \Gamma]n\}}{1 + (I_{SP}/I_{e,i})[\exp\{[g_{0MAX}(1-\Gamma) - \Gamma]n\} - 1]} \\ I_{e,i} = \frac{2}{\pi} \frac{1-\Gamma}{\Gamma} g_{0MAX} \left\{ 1 - \exp\left[-\frac{1.8}{1+g_{0MAX}} \frac{g_{0MAX}(1-\Gamma) - \Gamma}{\Gamma}\right] \right\} I_{SAT} \end{array} \right. \quad (7)$$

where $N_{eq} = L/(2\gamma^2\lambda_C) \sim 7.3$ represents the equivalent value of the number of undulator periods in Cerenkov FELs; $I_{SAT} \sim 7.4 \cdot 10^6$ [W] expresses the saturation power value related to the gain of the device (conventionally, the intensity is used instead of power, however,

in this case, the radiation transverse cross-section is a constant due to the presence of a waveguide, making power and intensity interchangeable); n indicates the round-trip number; $I_{AV} \sim 17,000 \text{ A}$ indicates the Alfvén current; Γ represent the total losses in the radiation resonator; I_{SP} expresses the spontaneous emission power of all the electrons in the bunch and integrated over the bandwidth; $I_{e,i}$ refers to the intracavity equilibrium power, and finally, g_{0MAX} indicates the maximum value of the small-gain, small-signal gain coefficient as a function of frequency [15]. The relevant parameters for the gain calculation are reported in Table 2.

Table 2. Cerenkov FEL Gain Parameters @ $\lambda = 250 \text{ }\mu\text{m}$.

Cerenkov FEL Gain Parameters @ $\lambda = 250 \text{ }\mu\text{m}$					
Electron Bunch Current	Angular Distribution	Transverse Distribution	Peak Gain Coefficient	Total Resonator Losses	Intracavity Equilibrium Power
$I_0 = 20.0$	$\sigma' = 5 \times 10^{-4}$ (r.m.s.)	$\sigma_x = 1 \text{ mm}$ (r.m.s.)	$g_{0MAX} = 0.4$	$\Gamma = 0.042$	$I_{e,i} = 7.22 \times 10^7 \text{ W}$

The behaviour of Equation (7) is reported in Figure 3a) for the gain expressions, G_I and G_{II} , as a function of the round trip number n , and in Figure 3b) for the ongoing power radiation, I_n and $I(n)$, again with respect to the round trip. The main result, as can be deduced from Figure 3, is that saturation is reached after about $n = 100$ round trips considering both methods reported in Equation (7). Considering the resonator length, as indicated in Table 1, we can deduce that saturation is gained in about $T_{SAT} \sim 200 \text{ ns}$, which is quite a short time with respect to the conventional macro-bunch duration of electron pulses generated by RF accelerators in the S-band ($\sim 3 \text{ GHz}$), which of the order of several microseconds. This will be relevant for the analysis of the velocity modulation induced on the remaining part of the macro-bunch itself.

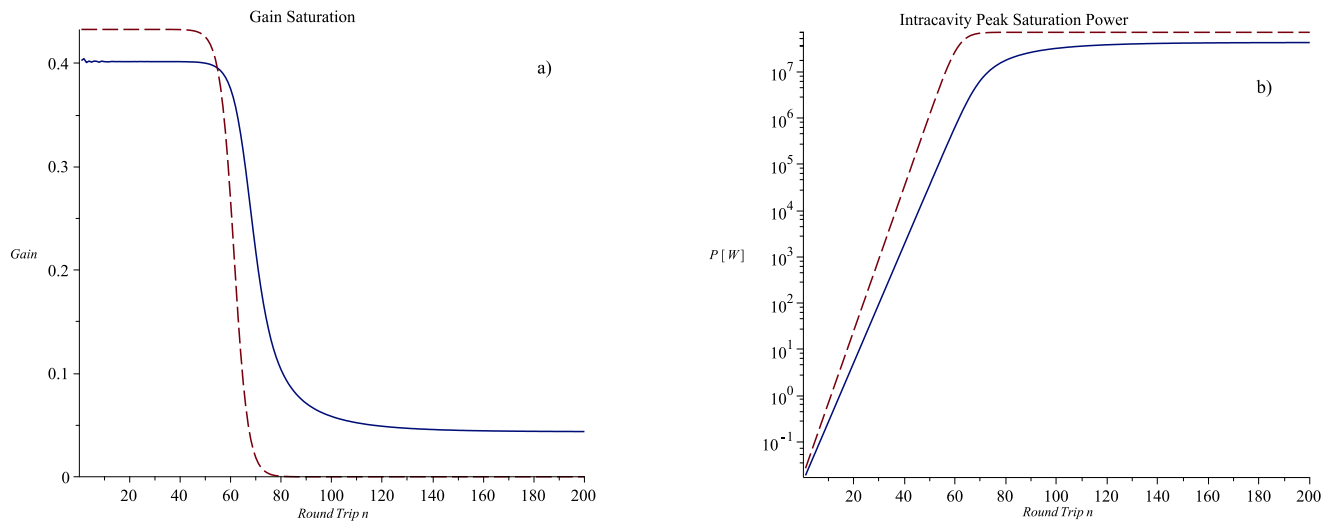


Figure 3. Saturation behaviour: (a) gain as a function of the round-trip number; and (b) intracavity power as a function of the round-trip number.

The peak intra-cavity peak power, as deduced by Figure 3b), is about $P_{SAT} \sim 4.2 \times 10^7 \text{ W}$; considering an average transverse radiation dimensions, obtained from the data reported in Table 1, of about $\Sigma_L = 1 \text{ cm}^2$, the electric field associated to the intracavity radiation at saturation is:

$$E_{SAT} = \sqrt{2I_{SAT}/(\epsilon_0 c \Sigma_L)} \approx 1.782 \cdot 10^7 [\text{V/m}]$$

Before analysing the dynamical process, it is worth briefly addressing the question of the longitudinal modes in the Cerenkov FEL resonator. The wavenumber mode separation, as evident from Equation (6), is $(\Delta\omega/c) = \pi/L$. The relative gain bandwidth is [11,15]:

$$\frac{\Delta\omega_G}{\omega} \approx \frac{1}{4N_{eq}} = \frac{\gamma^2\lambda_C}{2L} \Rightarrow \frac{\Delta\omega_G}{c} = \frac{\omega_C}{c} \frac{\gamma^2\lambda_C}{2L} \approx \frac{\pi\gamma^2}{L}$$

The number of modes contained in the gain bandwidth is therefore: $\Delta\omega_G/\Delta\omega = \gamma^2$. It is well known [11] that any FEL based on the RF accelerator locks all the longitudinal modes in a natural way. The result of such mode-locking is that a single short pulse of radiation travels back and forth inside the tuned resonator with a group velocity that is slightly smaller than that of the electron beam, causing a kind of anti-lethargic effect [23], unlike what happens for undulator FELs.

4. Electron Beam Modulation and Undulator Emission

At the end of the previous section, we saw how an intense electromagnetic pulse, that can be generated inside an optical resonator in about 200 nanoseconds, needs to be saturated. For electron macro-bunches, as long as few microseconds we will have thousands of micro-bunches available interacting with the electromagnetic field. If we analyse each of these electron micro-bunches, we recognise that, at the resonator entrance, each of them superimposes with a correspondent radiation micro-pulse as illustrated in Figure 4a). In such a situation, the electrons of the bunch, generally equally spaced in phase, will experience the oscillating longitudinal electric field E_z (Equation (6)) with a spatial periodicity of λ_C , as showed in Figure 4b). The situation represented in Figure 4 is quite similar to that of an electron beam accelerated by a series of RF cavities such as those of a standing-wave Linac [11,24]. The number of cavities can be estimated by calculating the number of the electric field oscillations “contained” within the electron micro-bunch length ($\delta z \sim \tau_e \beta_e c$) divided by the wavelength λ_C : $N_c \sim (\delta z/\lambda_C)$. The most widely used accelerators for FELs operate in the so-called S-band ($\nu_{RF} \sim 3$ GHz) and generate micro-bunches of a typical duration of $\tau_e \sim 15$ ps, which corresponds to a bunch length of about $\delta z \sim 5$ mm. Considering a radiation wavelength of $\lambda_C \sim 250 \mu\text{m}$, as for the example discussed in the previous sessions, we obtain $N_c \sim 20$.

It is possible, therefore, to imagine any optical cycle acting on the electrons in a way similar to that of the accelerating cavities of a Linac. We know, in fact, that electrons undergo to an energy variation that is connected to the particle-radiation relative phase. Such an energy variation will be positive for electrons close to the so-called accelerating phase and negative for those with an opposite phase. The result is a bunching of the electrons into N_c “slices”.

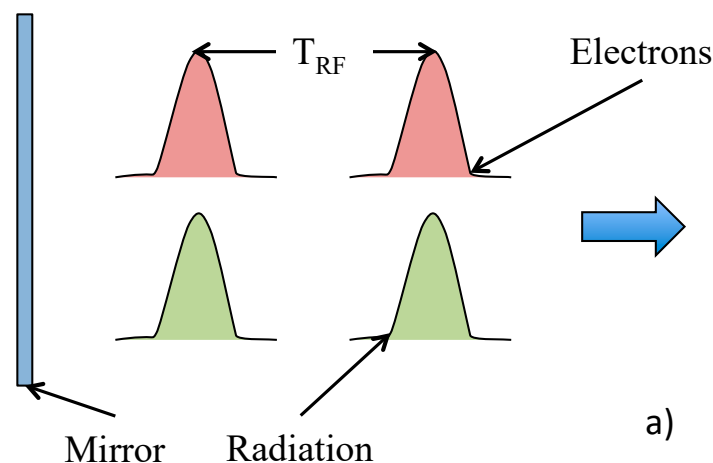


Figure 4. Cont.

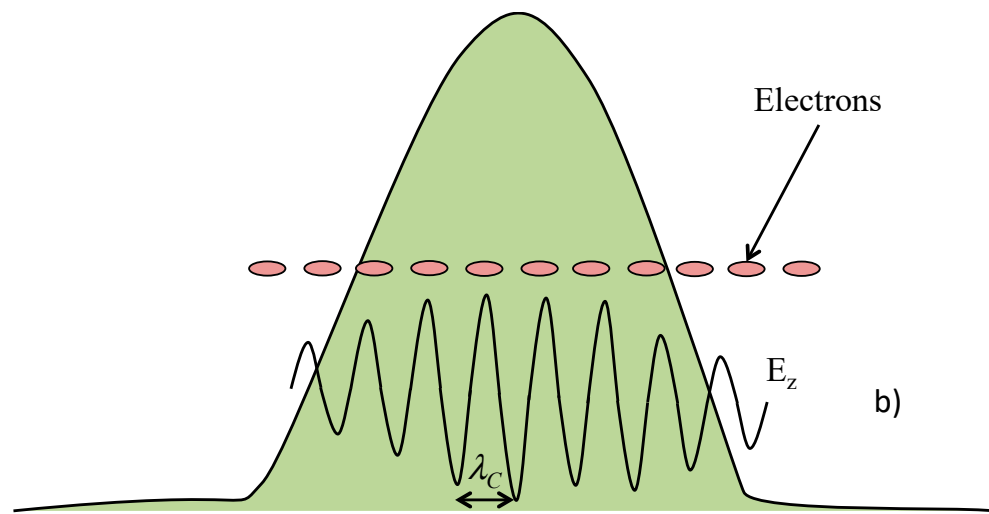


Figure 4. Electron bunch and radiation pulse interaction: (a) phase locking; and (b) electrons and radiation electric field interaction.

To properly evaluate the energy variation of a single electron, let us consider that the energy exchange occurs along the time needed for the electron, to cross the resonator length L . The particle, during this time $T = L/(c\beta_e)$, experiences a quasi-static electric field due to the fact that, even with small differences, its speed is almost synchronous with the electromagnetic pulse that travels with its group velocity $\beta_g = d(\omega/c)/dk$ (see Equation (5)), and therefore, $\beta_g \sim \beta_e$. The energy variation, for each electron, is consequently:

$$\Delta\gamma = \frac{\Delta E}{m_0c^2} = \frac{\mathbf{F} \cdot \mathbf{s}}{m_0c^2} = \int_0^T \frac{e\mathbf{E}(t)}{m_0c^2} \cdot \mathbf{v}_e dt = \frac{eE_{0z}}{m_0c^2} c\beta_e \int_0^T \cos(\omega t + \phi) dt \quad (8)$$

where the longitudinal electric field has been derived from Equation (6) and the constant term E_{0z} contains the transverse coupling between the electron and the evanescent field in the x direction. Before getting an explicit form for Equation (8), it is worth underlining that the phase ϕ usually refers to the RF field, at an angular frequency ω_{RF} , that accelerates the electron beam in the accelerator (Linac, for instance). In the present case, the phase ϕ should be referred to as the Cerenkov radiation field in the optical resonator, and therefore, ought to be “normalised” by means of the frequency ratio ω_C/ω_{RF} : $\phi \Rightarrow \phi(\omega_C/\omega_{RF}) = \phi(\lambda_{RF}/\lambda_C)$. After some algebra, we obtain:

$$\Delta\gamma = \frac{eE_{0z}}{m_0c^2} L \left[\frac{\sin\left(\frac{\omega}{c} \frac{L}{\beta_e}\right)}{\left(\frac{\omega}{c} \frac{L}{\beta_e}\right)} \cos\left(\phi \frac{\lambda_{RF}}{\lambda_C}\right) + \frac{\cos\left(\frac{\omega}{c} \frac{L}{\beta_e}\right)}{\left(\frac{\omega}{c} \frac{L}{\beta_e}\right)} \sin\left(\phi \frac{\lambda_{RF}}{\lambda_C}\right) \right] \quad (9)$$

The result of what has been discussed is that the energy modulation expressed by Equation (9) can be exploited to generate powerful radiation inside a magnetic undulator utilised as a radiator. The discussion after Equation (2) in Section 2 leads to a set of parameters, summarised in Table 3, for an undulator synchronous with the fundamental Cerenkov emission.

Table 3. Undulator–Radiator FEL Parameters @ $\lambda_U = 250 \mu\text{m}$.

Undulator–Radiator FEL Parameters @ $\lambda_U = 250 \mu\text{m}$					
Electron Energy	Undulator Period	Undulator Parameter	Number of Periods	Waveguide Width	Waveguide Height
$\gamma = 10.0$	$\lambda_w = 2.5 \text{ cm}$	$=1.0$	$N_U = 50$	$W = 0.5 \text{ cm}$	$H = 0.5 \text{ cm}$

The emission of radiation from a radiator by means of an ensemble of charged particles distributed in the phase space has been faced in the recent past [25,26]. To summarise some concepts, we can say that the electron beam, after the interaction, carries a modulation of the current \vec{J} that can be expressed as a Fourier expansion in terms of the harmonics l of the RF. Moreover, the electromagnetic field can be expanded in terms of the transverse modes, expressed by the aggregate index λ , of the waveguide that is needed to confine the radiation in the far infrared spectral range, and expressing the expansion coefficients as $A_{l,\lambda}$. Finally, the power $P_{l,\lambda}$, emitted due to the energy exchange between the electron beam and the radiation field in the magnetic field of the undulator, can be evaluated by means of the flux of the Poynting vector. Equation (10) summarises all the above in an extensive demonstration which can be found in [25] and the references therein:

$$\begin{aligned} \vec{J} &= \sum_{l=1}^{\infty} \vec{J}_l \exp(-i\omega_l t); \omega_l = 2\pi \frac{l}{T_{RF}} \\ A_{l,\lambda} &= -\frac{Z_0}{2\beta_g} \frac{e}{T_{RF}} \frac{KL}{\sqrt{\Sigma_\lambda}} \sum_{j=1}^{N_e} \frac{1}{\beta_{z,j} \gamma_j} \frac{\sin(\theta_{l,\lambda,j}/2)}{\theta_{l,\lambda,j}/2} i \exp\left(\frac{\theta_{l,\lambda,j}}{2} + l\psi_j\right); \theta_{l,\lambda,j} = \left(\frac{\omega_l}{c\beta_{z,j}} - \frac{2\pi}{\lambda_w} - k_\lambda\right) \\ P_{l,\lambda} &= \frac{\beta_g}{2Z_0} |A_{l,\lambda}|^2 \end{aligned} \tag{10}$$

where e is the electron charge, Z_0 is the vacuum impedance, Σ_λ is the radiation transverse mode size, N_e is the number of electrons contained in the bunch, $\beta_{z,j}$ is the longitudinal velocity of the j -th electron, β_g is the radiation group velocity and k_λ is the transverse mode momentum.

A brief analysis of Equation (10) tells us that the expansion coefficient $A_{l,\lambda}$ plays a significant function in the determination of the radiation formation. It is, in fact, the role of each electron in the bunch is relevant because it carries a specific energy γ_j and a specific phase ψ_j . In particular, the electron phase ψ_j , together with the interaction phase $\theta_{l,\lambda,j}$ enter in a more general phase term in $A_{l,\lambda}$ that, when summing up all of the contributions of the N_e electrons of the bunch, may generate constructive or destructive interactions. The maximum radiated power in the undulator is obtained when all the electrons contribute to the radiation formation with the same phase term (only depending on the harmonic number l), therefore, with an adequate distribution of the electrons in the phase-space.

What has been discussed, so far, about Equation (10), refers to the longitudinal properties of the particle–wave interaction, which concur with the undulator parameter K and period λ_w and the electron longitudinal velocities $\beta_{z,j}$. The transverse characteristics of the radiation emission are summarised by the mode aggregate index λ . It is evident, however, that the transverse space can play a role when the electron beam emittance values could be relevant for the radiation wavelength to be generated. A deeper and exhaustive analysis can be found in [27].

With such a mathematical background, an appropriate computational code was set up for the evaluation of the coherent generation of radiation in the undulator–radiator. The code is capable of evaluating the impact of an electron bunch, with a specific distribution in the phase-space, for the radiation generation, calculating the contribution of any electron, integrated along the interaction length. The code, at the moment, does not take into account saturation effects. The effect of the energy modulation introduced by the electron–field interaction inside the Cerenkov FEL optical resonator can be assessed by comparing the emission from an electron distribution $D(\gamma_j, \psi_j)$ and the same distribution to which an energy modulation is added $D(\gamma_j + \Delta\gamma(\psi_j)_j, \psi_j)$, where the contribution $\Delta\gamma(\psi_j)_j$ is calculated from Equation (9) for each electron. To this aim, an ad hoc electron distribution was generated in the phase-space having a uniform partitioning in energy with a total $\Delta\gamma = 0.2$ around $\gamma = 10$ (see Table 3) corresponding to a $\sigma_\gamma \approx 5 \cdot 10^{-3}$ r.m.s. The phase partitioning is again uniform, with an added Poissonian component, with a total $\Delta\psi = 20^\circ$ corresponding to the actual micro-bunch duration expressed as phase interval for Linac [11]. In Figure 5, we report the aforementioned electron distribution (Figure 5a) together with

the corresponding power spectrum (Figure 5b) calculated with Equation (10). The total power, integrated over the whole bandwidth, results in $P_{TOT} \sim 55$ W.

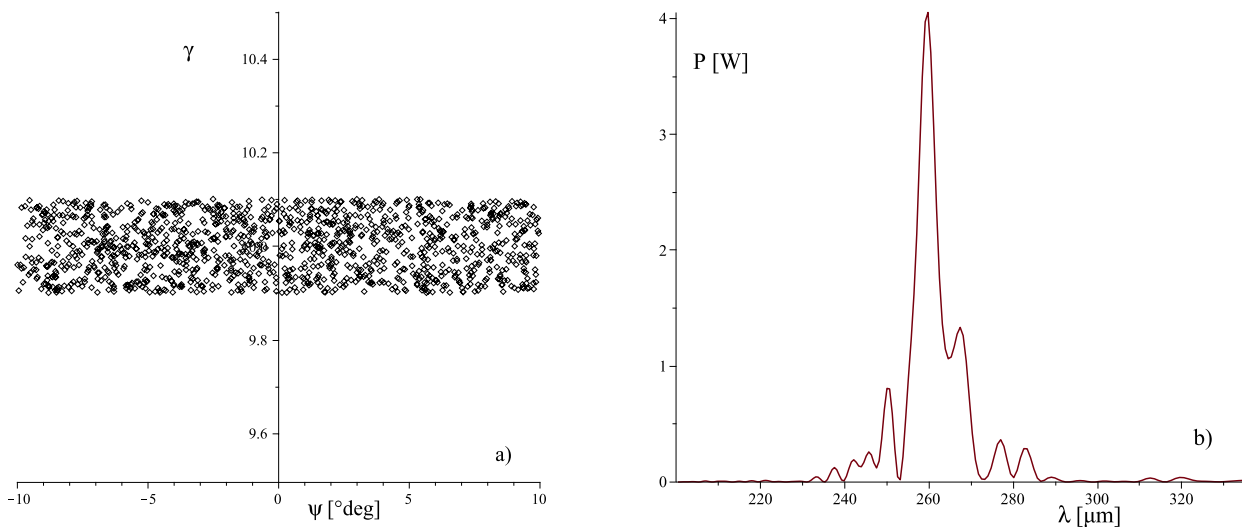


Figure 5. Emission by undulator-radiator: not the modulated case: (a) phase-space; and (b) power spectrum.

As anticipated, a similar calculation can be performed for the electron distribution of Figure 5a), to which the energy modulation $\Delta\gamma_j$ of Equation (9) is added for each electron of the distribution with its actual phase ψ_j and energy (through the velocity $\beta_{e,j}$). The amplitude of the electric field is the one evaluated at the end of Section 3 from the saturated intracavity radiation power $E_{0z} \sim 1.8 \times 10^7$ [V/m]. In Figure 6, we report the energy modulated electron distribution (Figure 6a) together with the corresponding power spectrum (Figure 6b), again calculated by means of Equation (10). As can be clearly seen, the emission is strongly increased by orders of magnitude due to the modulation introduced which, moreover, is not clearly distinguishable when looking at Figures 5a and 6a. It is further worth underlining how the total bandwidth is slightly reduced with respect to the unmodulated case. The total power, integrated over the whole bandwidth, now results as $P_{TOT} \sim 1.28 \times 10^7$ W.

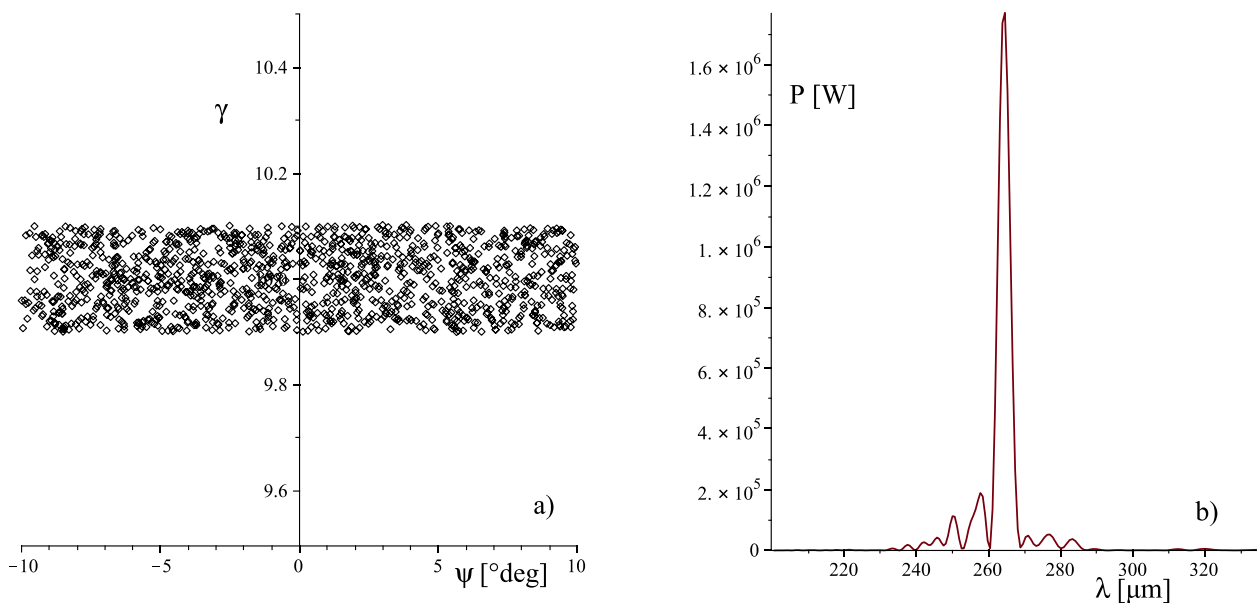


Figure 6. Emission by undulator-radiator: modulated case: (a) phase-space; and (b) power spectrum.

We may now ask whether there is any optimisation procedure to further increase the power radiated by the undulator. The most relevant tool is the distance between the Cerenkov electromagnetic resonator and the entrance of the magnetic undulator. This is because the energy modulation acquired by the electrons in the cavity transforms into a velocity modulation, and consequently bunches before entering the undulator interaction region. This “drift space” allows a ballistic process that correlates the velocity variation of each electron, with its position, and therefore phase, in the bunch. In Equation (11), we report the phase term that should be inserted in the set of Equation (10) that takes into account the phase variation, after the velocity modulation expressed by $(v_z)_j$ and for a specific drift space L_{Drift} . The index “ j ” indicates the specific electron and v_{ref} is the velocity of the “reference electron”:

$$\left(\Psi_{Drift}\right)_j = \omega_{RF} L_{Drift} \left(\frac{1}{(v_z)_j} - \frac{1}{v_{ref}} \right) + \psi_j \quad (11)$$

Considering a series of values for L_{Drift} ranging from 0 to 3.5 metres, the power spectrum was calculated and reported in Figure 7. As can be appreciated, the peak power, starting from a specific value, tends to reduce, while increasing L_{Drift} , and the spectrum itself tends to broaden with a couple of peaks appearing. A further increase in the modulator radiator distance produces a spectral band reduction and a peak power increase up to the final value.

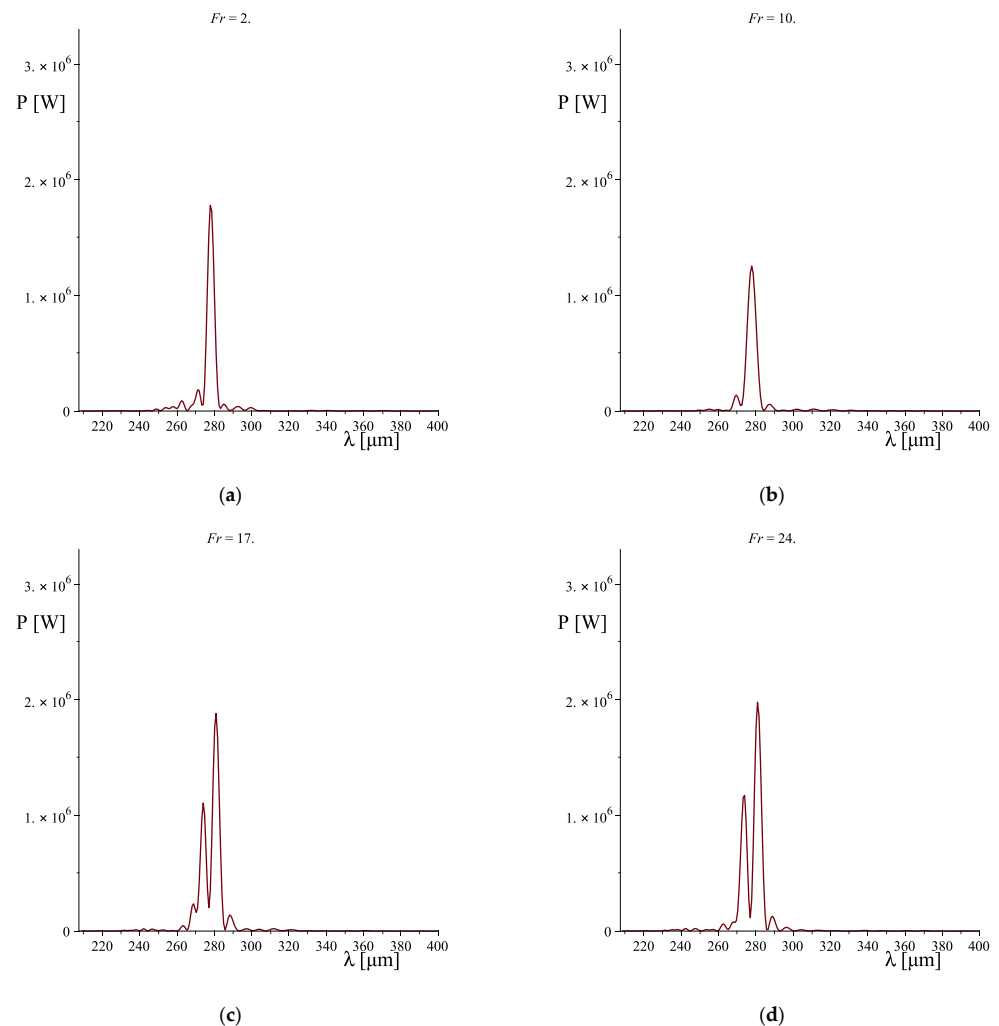


Figure 7. Cont.

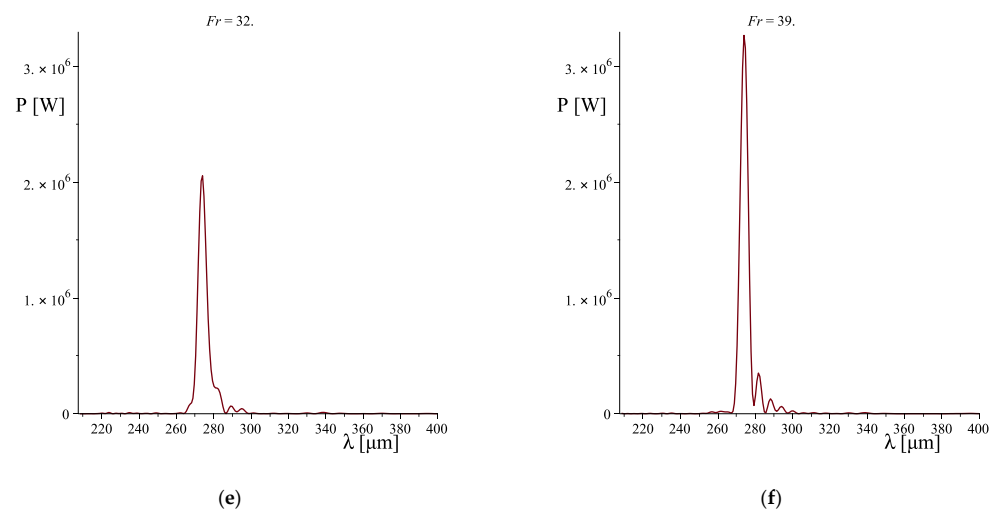


Figure 7. Power spectrum for different drift-space values: (a) $L_{Drift} = 0.18$ m; (b) $L_{Drift} = 0.90$ m; (c) $L_{Drift} = 1.52$ m; (d) $L_{Drift} = 2.15$ m; (e) $L_{Drift} = 2.87$ m; and (f) $L_{Drift} = 3.50$ m.

5. Conclusions

The example reported to date indicates how a hybrid scheme for free electron devices can be effective for the power enhancement of the electromagnetic radiation generated. This two-elements scheme, based on an oscillator, in which intracavity radiation acts as an energy modulator, and a magnetic undulator as a radiator, is a versatile arrangement because the oscillator section can be chosen among a series of different devices. As anticipated, together with the Cerenkov device, other sources can be taken into account; among which the Smith–Purcell is an interesting choice because it offers characteristics that lay between that of a Cerenkov FEL (being a slow-wave device) and an undulator FEL (wavelength scales inversely with the electron energy, as can be seen in Equation (12)). The synchronic condition, in fact, results to be [10,28]:

$$\lambda_{SP} = \frac{\Lambda}{|n_{so}|} \left(\frac{1}{\beta_e} - \cos \theta \right) \quad (12)$$

where Λ represents the grating period, n_{so} indicates the grating spectral order and θ is the angle between the electron beam direction (parallel to the grating surface) and the observer. A new parameter, in the Smith–Purcell-based FEL, is evident from Equation (12) and is the angle θ that offers a wide and continuous range of spectral tunability [28] that can be exploited, keeping fixed other parameters like the electron energy and the grating geometry. This characteristic increases the flexibility of the hybrid scheme FEL because it easily allows to obtaining the condition $\lambda_U = \lambda_{SP}/n$, where $n = 1, 2, \dots$, because the $\cos \theta$ term can be used to obtain the maximum wavelength extension:

$$\lambda_{SP}^{(+)} = \frac{\Lambda}{|n_{so}|} \frac{1}{\beta_e} \Rightarrow \lambda_{SP}^{(-)} = \frac{\Lambda}{|n_{so}|} \left(\frac{1 - \beta_e}{\beta_e} \right).$$

The harmonic number n is, therefore, a pivotal parameter for extending the spectral emission of such a coherent source [5–7], that with a proper combination of all the parameters involved, for both the oscillator and the radiator, prove to be a promising and versatile device, with the additional feature of compactness.

Funding: This research received no external funding.

Institutional Review Board Statement: Not applicable.

Informed Consent Statement: Not applicable.

Data Availability Statement: Not applicable.

Conflicts of Interest: The authors declare no conflict of interest.

References

1. Pantell, R.H.; Soncini, G.; Puthoff, H.E. Stimulated photon-electron scattering. *IEEE J. Quantum Electron.* **1968**, *QE-4*, 905–907. [[CrossRef](#)]
2. Deacon, D.A.G.; Elias, L.R.; Madey, J.M.J.; Ramian, G.J.; Schwettman, H.A.; Smith, T.I. First Operation of a Free-Electron Laser. *Phys. Rev. Lett.* **1977**, *38*, 892–894. [[CrossRef](#)]
3. van Amersfoort, P.W.; Bakker, R.J.; Bekkers, J.B.; Best, R.W.B.; van Buuren, R.; Delmee, P.F.M.; Faatz, B.; van der Geer, C.A.J.; Jaroszynski, D.A.; Manintveld, P.; et al. First lasing with FELIX. *Nucl. Instr. Meth.* **1992**, *A318*, 42–46. [[CrossRef](#)]
4. Milton, S.V.; Gluskin, E.; Arnold, N.D.; Benson, C.; Berg, W.; Biedron, S.G.; Borland, M.; Chae, Y.C.; Dejus, R.J.; Den Hartog, P.K.; et al. Exponential gain and saturation of a self-amplified spontaneous emission free-electron laser. *Science* **2001**, *292*, 2037–2040. [[CrossRef](#)] [[PubMed](#)]
5. Bonifacio, R.; De Salvo Souza, L.; Pierini, P.; Scharlemann, E.T. Generation of XUV Light by Resonant Frequency Tripling in a two Wiggler FEL Amplifier. *Nucl. Instr. Meth.* **1990**, *A296*, 787–790. [[CrossRef](#)]
6. Dattoli, G.; Doria, A.; Giannessi, L.; Ottaviani, P.L. Bunching and exotic undulator configurations in SASE FELs. *Nucl. Instr. Meth.* **2003**, *A507*, 388–391. [[CrossRef](#)]
7. Ciocci, F.; Dattoli, G.; De Angelis, A.; Faatz, B.; Garosi, F.; Giannessi, L.; Ottaviani, P.L.; Torre, A. Design Considerations on a High-Power VUV FEL. *IEEE J. Quantum Electron.* **1995**, *QE-31*, 1242–1252. [[CrossRef](#)]
8. Asgekar, V.; Dattoli, G. Hybrid free electron laser devices. *J. Appl. Phys.* **2007**, *101*, 063111-1–063111-4. [[CrossRef](#)]
9. Ciocci, F.; Dattoli, G.; Doria, A.; Schettini, G.; Torre, A.; Walsh, J.E. Spontaneous Emission in Cerenkov FEL Devices: A Preliminary Theoretical Analysis. *Il Nuovo Cimento* **1988**, *10D*, 1–20. [[CrossRef](#)]
10. Urata, J.; Goldstein, M.; Kimmitt, M.F.; Naumov, A.; Platt, C.; Walsh, J.E. Superradiant Smith-Purcell Emission. *Phys. Rev. Lett.* **1998**, *80*, 516–519. [[CrossRef](#)]
11. Dattoli, G.; Doria, A.; Sabia, E.; Artioli, M. *Charged Beam Dynamics, Particle Accelerators and Free Electron Lasers*, 1st ed.; IOP Publishing Ltd.: Bristol, UK, 2017.
12. Roberts, S.; Coon, D.D. Far-Infrared Properties of Quartz and Sapphire. *J. Opt. Soc. Am.* **1962**, *52*, 1023–1029. [[CrossRef](#)]
13. Collin, R.E. *Foundations of Microwave Engineering*; McGraw-Hill: Singapore, 1966.
14. Walsh, J.E. Stimulated Cerenkov Radiation. *Adv. Electron. Electron Phys.* **1982**, *58*, 271–310.
15. Dattoli, G.; Doria, A.; Gallerano, G.P.; Renieri, A.; Schettini, G.; Torre, A. A Single-Particle Calculation of the FEL-Cerenkov Gain. *Il Nuovo Cim.* **1988**, *101B*, 79–84. [[CrossRef](#)]
16. Ciocci, F.; Dattoli, G.; Doria, A.; Gallerano, G.P.; Schettini, G.; Torre, A. Spontaneous Emission in a Double Dielectric Slab for Cerenkov Free-Electron-Laser Operation. *Phys. Rev. A* **1987**, *36*, 207–210. [[CrossRef](#)] [[PubMed](#)]
17. Dattoli, G. Logistic function and evolution of free-electron-laser oscillators. *J. Appl. Phys.* **1998**, *84*, 2393–2398. [[CrossRef](#)]
18. Andrews, H.L.; Brau, C.A. Three-dimensional theory of the Cerenkov free-electron laser. *J. Appl. Phys.* **2007**, *101*, 104904-1–104904-6. [[CrossRef](#)]
19. Rigrod, W.W. Gain Saturation and Output Power of Optical Masers. *J. Appl. Phys.* **1963**, *34*, 2602–2603. [[CrossRef](#)]
20. Herman, A.H. Theory of mode locking with a fast saturable absorber. *J. Appl. Phys.* **1975**, *46*, 3049–3058.
21. Dattoli, G.; Cabrini, S.; Giannessi, L. Simple model of gain saturation in free-electron lasers. *Phys. Rev. A* **1991**, *44*, 8433–8434. [[CrossRef](#)]
22. Dattoli, G.; Giannessi, L.; Ottaviani, P.L.; Carpanese, M. A simple model of gain saturation in high gain single pass free electron lasers. *Nucl. Instr. Meth.* **1997**, *A393*, 133–136. [[CrossRef](#)]
23. Dattoli, G.; Doria, A.; Gallerano, G.P.; Schettini, G.; Torre, A.; Walsh, J.E. Pulse Propagation Theory for the Cerenkov Free-Electron Laser. *Il Nuovo Cim.* **1989**, *103B*, 281–289. [[CrossRef](#)]
24. Wangler, T.P. *Introduction to Linear Accelerator Theory*; LAUR-93-805; Los Alamos National Laboratory: Washington, DC, USA, 1993.
25. Doria, A.; Gallerano, G.P.; Giovenale, E.; Letardi, S.; Messina, G.; Ronsivalle, C. Enhancement of Coherent Emission by Energy-Phase Correlation in a Bunched Electron Beam. *Phys. Rev. Lett.* **1998**, *80*, 2841–2844, and references therein. [[CrossRef](#)]
26. Doria, A.; Gallerano, G.P.; Giovenale, E. Novel Schemes for Compact FELs in the THz Region. *Condens. Matter* **2019**, *4*, 90. [[CrossRef](#)]
27. Bahrtdt, J. Shaping Photon Beams with Undulators and Wigglers. In *Synchrotron Light Sources Free Electron Lasers*; Springer: Berlin/Heidelberg, Germany, 2016; pp. 751–819.
28. Doucas, G.; Kimmitt, M.F.; Doria, A.; Gallerano, G.P.; Giovenale, E.; Messina, G.; Andrews, H.L.; Brownell, J.H. Determination of longitudinal bunch shape by means of coherent Smith-Purcell radiation. *Phys. Rev. Accel. Beams* **2002**, *5*, 072802-1–072802-8. [[CrossRef](#)]